EXAMENSARBETE INOM ELEKTROTEKNIK,
AVANCERAD NIVÅ, 30 HP

STOCKHOLM, *SVERIGE 2018*

Physical Layer Algorithms for Intrabody Nano-Communications

ANDERS ENQVIST

KTH
SKOLAN FÖR ELEKTROTEKNIK OCH DATAVETENSKAP

Physical Layer Algorithms for Intrabody Nano-Communications

ANDERS ENQVIST

Master in Wireless Systems
Date: November 7, 2018
Supervisor: Hamed Farhadi, Nafiseh Shariati, Mikael Johansson
Examiner: Gabor Fodor
Swedish title: Det fysiska lagrets algoritmer för nanokommunikation i människokroppen
School of Electrical Engineering and Computer Science

Abstract

In this thesis we develop a mathematical model of the physical layer for an in-body nano-machine (NM) communication. The purpose is finding what modulation and detection schemes are suitable for application in the body and discovering what factors limit the feasible communication distance. Inside the body, the NMs use small antennas operating in the THz frequency spectrum. They have limited energy resources and low computational power and must fulfill their task in a challenging environment with large absorption losses. By employing on-off-keying pulse modulation and small integrating receiver circuits, it is possible to consume minimal energy while being able communicate over small distances of a few mms. This is shown through a simulation of a point to point nano-communication link. We also demonstrate how connecting several NMs in a network and employing amplify-and-forward relaying can facilitate communication over larger distances. The final analysis shows that communication inside the body is possible over short distances, a few mms at most, but transmitting a signal strong enough to connect a NM network to an external terminal may prove challenging.

Sammanfattning

Det här examensarbetet beskriver en matematisk model av det fysiska lagret för kommunikation mellan nano maskiner i människokroppen. Syftet är att fastställa vilka typer av modulations- och detektionsalgoritmer som är möjliga att använda och att förstå vilka faktorer som begränsar möjligheten för nanomaskiner att kommunicera över längre avstånd. Nanomaskinerna använder mycket små antenner i terahertzspektrumet. De har väldigt begränsade energiresurser, liten beräkningskraft och måste kunna fungera i en utmanande miljö med stora absorptionsförluster. Genom att använda sig av On-Off-Keying, pulsmodulering och små integrationskretsar går det att kommunicera över små avstånd i storleksordningen några mm och fortfarande använda väldigt lite energi. Detta visas genom en simulering av en kommunikationslänk mellan två nanomaskiner. Vi demonstrerar även hur man genom att koppla ihop flera nanomaskiner i ett nätverk och använda sig av Amplify-and-Forward reläer kan kommunicera över större avstånd. Slutsatsen av arbetet är att det är möjligt för nanomaskiner i kroppen att kommunicera över korta avstånd i storleksordningen några mm. Att skicka en signal stark nog för att möjliggöra ett nanonätverk att trådlöst kommunicera med en terminal utanför kroppen är dock en uppgift som blir svår att lösa.

Acknowledgements

Firstly, I would like to thank my supervisor, Prof. Gabor Fodor, for giving me an opportunity to pursue my masters degree at Ericsson in the exciting field of nano-communications. His work ethics and expertise make him an excellent role model to follow in my future career.

I extend my sincerest gratitude to my supervisor, Dr. Hamed Farhadi, for sharing with me his knowledge, experience and skills. I am especially thankful to him for numerous discussions, valuable advice, constructive criticism and his attention to detail.

I would like to thank my friends for their encouragement and my parents for their support. A special gratitude goes out to my lovely wife Julia for always believing in me and my daughter Isabelle for always making me smile.

Contents

Chapter 1

Introduction

1.1 Background

The idea of molecular communications or nano-networks, as a new paradigm for engineered biological (in-vivo) nanomachines (NMs) that communicate with each other and with natural biological systems, is attracting increasing research attention and raises commercial interests[16]. It is expected that in the near future it will be possible to implant engineered NMs into a closed environment such as the human body. There they can perform simple but important tasks of actuation, sensing and computation. The concept of NMs include purified protein molecules, genetically bio-engineered cells, artificial protocells and bio-silicon hybrid devices. They can interact with existing biological systems to enable new important functions such as delivering medicine, forming bio-sensing networks measuring important health care parameters (for example glucose levels and ocular pressure) and forming actuator networks [5]. A network of NMs communicating using electromagnetic waves is often referred to as a wireless nano-sensor network (WNSN).

The NMs will need to be able to communicate with each other inside the body in order for them to fulfill their functions. There are several possible ways of making NMs communicate such as molecular communication which is similar to how cells in the body naturally communicate or acoustic communication using sound waves. The theory of electromagnetic communication and system design however is the most developed one. It has the advantage of making it easy to propose ideas and evaluate the performance of the electromagnetic com-

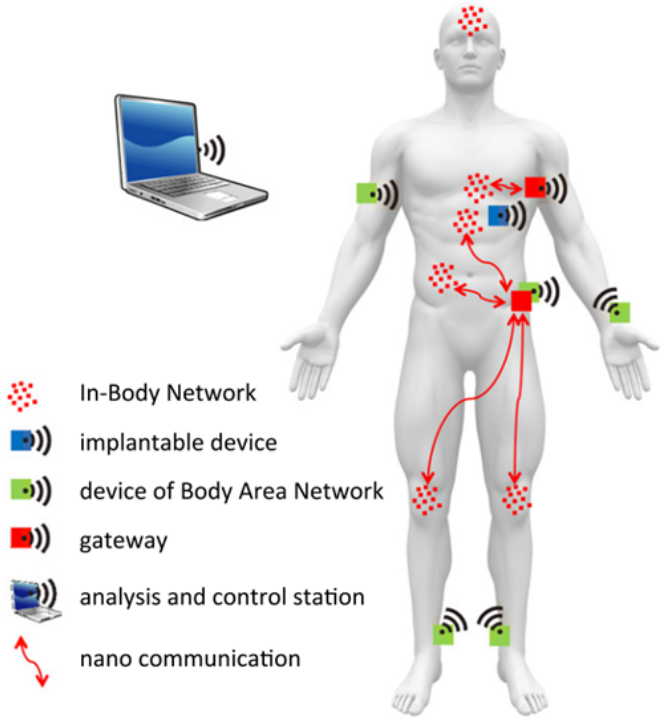

Figure 1.1: It is envisioned that in the future nano-networks will be able to perform important medical functions inside the body and communicate with an external terminal.

munication system. Although using electromagnetic waves is attractive, existing wireless technology must be adopted to the nanoscale environment [4]. This introduces constraints on available computational and transmission power due to the requirements on device and antenna size of the NMs, their limited energy budget and the frequency bands that may be used for nanoscale communication[15]. The modulation and signal detection techniques used although similar to already existing wireless technologies require new systems to be designed to work on the nanoscale. In this project we explore how the NMs may be able to communicate to each other. The WNSN could perhaps also communicate to devices located on or outside the body (such as a smart phone or a laptop) in order to transmit data to a user and to receive information and commands from control units. An image of a connected WNSN which enables future medical IoT applications is shown in figure 1.1.

1.2 Problem Formulation

In this project we help develop an electromagnetic wave-based way of communication between NMs inside the human body. We explore if and how it is possible to transmit information between in-body NMs and outside-the-body devices. To this end we aim to answer the following questions: What are the constraints imposed on the physical layer in NM communications and what is required of an algorithm to be applicable to NMs? How do we best design the modulation, signal detection and channel coding to work on the nano-scale? Is it possible to make the NMs work together and use cooperative transmission schemes to connect a WNSN to an external device?

1.3 Goals

The goal of the thesis is to design signal transmission and reception techniques which work on the nanoscale and classify the performances of different physical layer algorithms. To do this, a mathematical model of communication between NMs must be developed. A simulation environment in Matlab of this mathematical model is used to numerically evaluate the performance of the suggested communication scheme.

An expected deliverable of the project is a mathematical model of communication between NMs inside the body and from NMs inside the body to external terminals. A Matlab simulation environment of this model will be created in order to test the performance of promising physical layer algorithms. The performance of the physical layer algorithms will be evaluated using performance metrics such as signal-to-noise ratio (SNR), bit error rate (BER) and energy efficiency.

1.3.1 Benefits, Ethics and Sustainability

This thesis presents research at a very early development stage. There are no networks of operational nano-machines. However generation of motion, molecule detection and measurements inside a person may be performed by NMs and it is envisioned that this will create new possibilities for future nano-medical applications. The outcome of this project is likely to benefit developers of NMs and companies responsible for the communication networks of NMs. Exactly how NMs and WNSNs in the future will come to benefit mankind remains to be seen.

1.4 Methodology

The work was carried out at Ericsson Radio Research and at the Department of Automatic Control of KTH Royal Institute of Technology. Nano-communications is a relatively new research area and this thesis is a theoretical study of applicable methods for electromagnetic communication. In order to investigate the nano- communication system a mathematical model depicting a nano- communication link or a nano-communication network is created and implemented in Matlab. The numerical results of the simulations are then used to evaluate the performance of the proposed algorithms. The propagation channel models used herein are derived from relevant research papers and our results depend on their validity. However, our physical layer algorithms are often taken from different areas of digital communications before adopting them to the nano-scale.

1.5 A Note on The Scope of the Present Thesis Report

The scope of this thesis is rather broad because the concept of physical layer algorithms contain several different parts. We use existing channel models of certain tissues of the human body at specific Terahertz bandwidths. Assumptions on NM capabilities have been developed by others and are postulated. The scope of this thesis is point-to-point communication link and relay network. It is an early stage feasibility study of a NM communication system, but the simulations are restricted to not include interference between nano-machines. Deductive reasoning is sometimes used to motivate how a system parameter might influence or can be influenced by the interference in the system, although the numerical investigation of this issue is outside the scope of this thesis.

1.6 Outline

The different parts of a nano-communication system make up the chapters of the thesis. In Chapter 2 we will discuss theoretical background material that is essential to understanding the thesis. This includes

the physical capabilities of the nano-machines and the channel model. Both are needed in order to understand the physical layer algorithms but they are not a subject of investigation in the thesis. In Chapter 3 the design of a point-to-point nano-communication link is set up. We discuss the channel model, signal modulation and detection algorithms in details, and simulate the link in Matlab. In Chapter 4 we discuss networks of NMs and the feasibility of cooperative communication schemes using nano relays to improve the system performance, where NMs are enabled to connect to external devices. General conclusions and suggestions for future work are made in Chapter 5.

Chapter 2

Theoretical Background

2.1 Modulation

The transfer of information in wireless nano-sensor networks is conveyed through the process of modulation. Because of the small size of the nano-machines and due to the recent developments in graphene based antennas, electromagnetic transmission in the THz frequency band is seen as a feasible option. The motivation for using THz frequencies for communication between NMs is the fact that reducing the size of an antenna down to a few hundreds of nanometers leads to extremely high operating frequencies. New nano-antennas based on graphene can have resonant frequencies up to two orders of magnitude below that of nano-antennas fabricated with other materials. Studies point to the THz band (0.1-10 THz) as the frequency range of operation of these novel nano-antennas. These frequency bands are currently unallocated and can potentially support very high capacities due to the available wide bandwidth [2]. However, nano-machines are very simple, and therefore the modulation and demodulation of communication between nano-machines have to be very simple. In addition, in-vivo communication at the THz band is limited in range due to the large path loss which drastically reduces the received signal power and limits the possible communication distance to some millimeters.

When designing a communication system, it is important that the system is efficient not just in general but for its intended purpose. This means that each communication system has a different set of requirements and restrictions to account for. For most wireless systems, such as telecommunication networks, there are often many users who have

to share a limited bandwidth with each other. This means that each user in the network needs to communicate in a spectrally efficient way to achieve the highest possible reliable transmission rates by exploiting the available radio resources. This is a well developed research field and many advanced modulation techniques such as quadrature amplitude modulation (QAM) and orthogonal frequency division multiplexing (OFDM) exist that can push the bit-rate to the limit while limiting the interference. However, such techniques – while spectrally efficient – are computationally demanding and not always power efficient. This is because they rely on using sinusoidal waves of certain frequencies to transmit the information. Unfortunately, it takes a lot of energy to continuously transmit sinusoidal waveforms.

For a WNSN operating in the THz frequency band the situation is different. There is a huge bandwidth available and external users will not be interfering with the network and the network itself will not interfere with others. A problem is that the NMs have limited energy reserves and low computational power and therefore require a simple but power efficient transmission scheme.

2.1.1 On-Off Keying

We are – in accordance with other research papers – suggesting using pulse based modulation techniques for communication in WNSNs [10]. The communication channel of the human body differs from that of air, not only in the attenuation of the signal due to the path loss, but also because the molecules present in the body absorb a lot of the transmitted signal energy and then re-radiate it into the body, effectively creating an induced noise source. Because of this induced noise, impulse-based modulation schemes are seen as promising candidates. This is because the re-radiation of the energy caused by the molecules will interfere with sine-wave carriers. However, pulse-based communication systems using on-off-keying (OOK) are resistant to this phenomenon, since the extra noise only occurs when transmitting a pulse, but not when being silent. This will be discussed in greater detail in Chapter 3.

2.1.2 Energy Efficiency

A pulse is a signal of very limited time duration. The more time limited the pulse, the more bandwidth it occupies. Because we are operating in the THz frequency band inside the body, we may employ pulses of duration in the order of picoseconds. Such short pulses are naturally energy efficient, and can be stacked densely, which allows for communication rates of several Gbit/s[11]. It should be noted that OOK is preferred over BPSK from an energy efficiency (and also complexity) perspective, because whenever the transmitter is staying silent when transmitting a zero, it is not consuming energy. One reason for requiring energy efficient communication inside the body is the limited energy resources of the NMs as already discussed. Another reason for imposing the requirement of energy efficiency is the safety constraints for inside the body communications due to heating and radiation. It will be discussed in the following section.

2.1.3 Human Body Heating

A potential issue and reason as to why in-vivo networks have to be energy efficient is that we need to ensure that the tissues in the body surrounding the NMs are kept at body temperature. Because the NMs are to be installed inside the body, radiated energy will cause heating and may potentially damage the tissues if the radiated energy exceeds certain thresholds. If the temperature at a certain area inside the body rises we risk harming it. Pulse-based communication also minimizes the impact because the energy in a single pulse is generally very low due to its short time-duration of only a fraction of a pico-second. It is shown how the heating of the human body could be an issue when transmitting a continuous wave of high power but for OOK the temperature increase is kept at acceptable levels [6].

2.2 Physical Capabilities

Nano-machines are very small devices: up to a few cubic μm large [2]. Because of their small size, their energy reserves are severely limited and the physical layer algorithms have to be energy efficient. It is likely that NMs will be able to harvest energy inside the body. Potential energy sources include human body movement, biochemical com-

pounds, ambient radiation or small temperature gradients. All methods are described in [13]. Recent progress made in the antenna technology area makes it possible to implement small antennas on NMs. In this thesis, we are – in accordance with others – assuming that the NMs are capable of transmitting short pulses in the low part of the THz band [11]. Their energy is limited in the range of pJ[17]. To keep our results realistic, we impose the following restrictions on NMs:

- energy transmitted per pulse is 1 pJ
- operational bandwidth B is 0.5 to 1.5 THz

Chapter 3

Nano-Communication Link Design

3.1 Introduction

In this chapter we present the human body channel model for signal propagation in the nano-network and discuss how to model the noise. We further investigate suitable modulation and detection techniques that may be used in the physical layer for communication between NMs. Lastly we conduct a link-level simulation of the communication between two NMs and evaluate the performance of our proposed solutions.

3.2 Human Body Channel Model

The human body channel model at THz frequencies remains largely unexplored with many details yet to uncover. We are using the channel model presented in [19]. It is described how transmitted electromagnetic waves suffer a loss due to two factors. Firstly the signal is attenuated as the power is spherically propagated outwards from the isotropically radiating antenna. Secondly, part of the signal is absorbed by various organic molecules in the body. In-body communication at THz frequencies is primarily limited in range due to the high absorption loss. In general, irrespectively of the type of tissue of the body, the loss is high enough to allow propagation at distances of at most a few mm before the signal has been lost. For our pur-

poses, we are restricting the analysis to propagation inside human blood. The reason for this is that blood offers the harshest propagation conditions due to its very high signal absorption coefficient, and we can conclude that a particular physical layer algorithm of choice will perform in other tissue types if it works in blood. The molecular absorption in blood at the THz band is characterized by the absorption coefficient α. Reference [17] gives measurements of the absorption coefficients between 0.5 and 1.5 THz. By looking at the measurement data in Figure 3.1, it is clear that the absorption coefficient shows a roughly linear increase with frequency. We have therefore decided to model $\alpha(f)$ by fitting a straight line by means of the least square error method through the measurement points. In the bandwidth B of 0.5 to 1.5 THz, the channel will be modeled as a band pass filter, allowing signals only within this frequency range to pass. This implies that the channel model is as follows

$$H(f) = \begin{cases} \frac{c}{4\pi nfr} e^{-\alpha(f)r} e^{-j2\pi fr/c} & \text{if } 0.5 < |f| < 1.5 \text{ THz} \\ 0, & \text{otherwise.} \end{cases} \tag{3.1}$$

3.3 Noise Model

We model the noise as the one presented in [18]. It is due to two factors. Firstly, there is a background radiation noise N_b. Secondly, part of the radiated signal energy is absorbed by molecules in the body and re-radiated as an additional source of noise $N_s(r)$ in the system.

The background noise in the system N_b is independent of the transmission distance and given by

$$N_b = \int_B B(T_0, f) \Big(\frac{c}{\sqrt{4\pi} n_0 f} \Big)^2 df. \tag{3.2}$$

It is assumed to be additive white Gaussian noise (AWGN). $n_0 = 1.97$ is the refractive index of blood and $T_0 = 310$ K is the human body temperature. $B(T_0, f)$ is Planck's function.

The self induced noise $N_s(r)$ is also be modeled as AWGN, because the many different molecules absorb and re-radiate energy independently of each other, thus causing $N_s(r)$ to have a Gaussian distribution [12]. Its power is given by

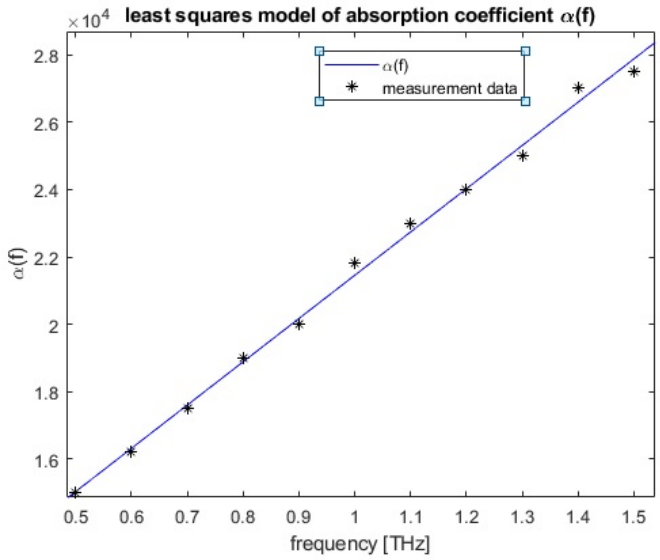

Figure 3.1: A least squares model of the absorption coefficient in human blood $\alpha(f)$.

$$N_s(r) = \int_B S(f)(1 - e^{-\alpha(f)r})\Big(\frac{c}{4\pi nfr}\Big)^2 df, \tag{3.3}$$

where $S(f) = P(f)P^*(f)$ is the power spectral density (PSD) of the transmitted signal $p(t)$. $P(f)$ is the Fourier transform of $p(t)$ and $P^*(f)$ its complex conjugate. The total noise in the system is equal to

$$N_M(r) = N_b + N_s(r). \tag{3.4}$$

Lastly, the received power is

$$P_{rx}(r) = \int_B S(f)(\frac{c}{4\pi nfr})^2 e^{-\alpha(f)r} df. \tag{3.5}$$

Only the background noise is present if no signal is transmitted. In Figure 3.3, the received signal and noise power are shown.

3.4 Pulse Shaping Design

It is possible to transmit power in the system more efficiently by designing a pulse $p(t)$ of a shape that matches the communication channel properties. The power-spectral-density $S(f)$ of the chosen pulse

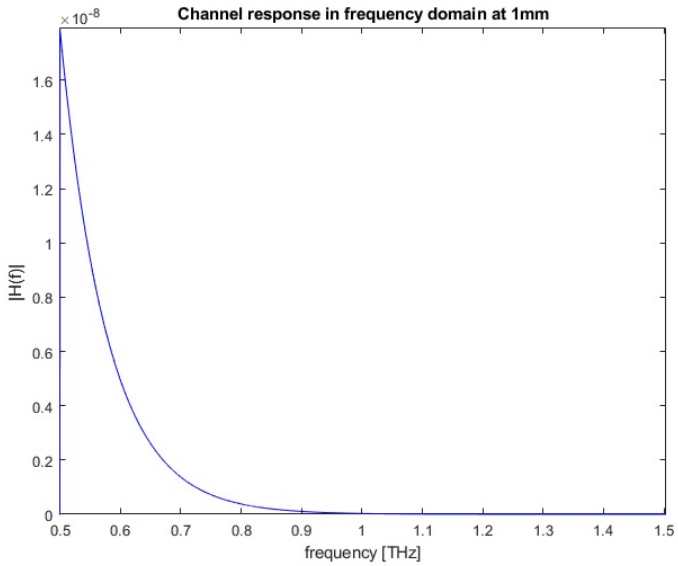

Figure 3.2: The nano channel model of human blood at a communication distance of 1 mm.

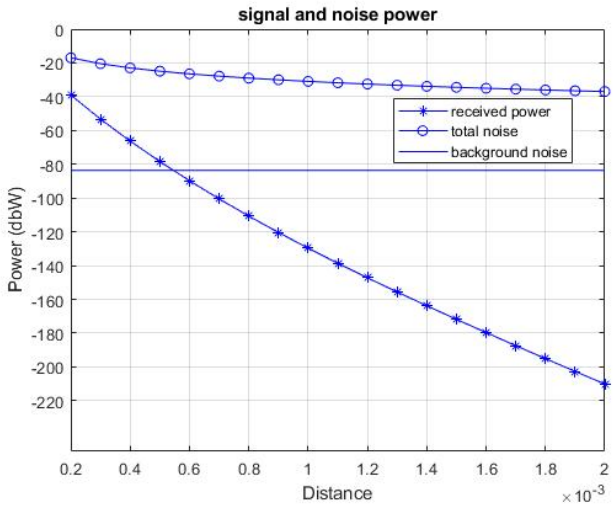

Figure 3.3: received signal and noise power vs distance for a pulse containing 1 pJ energy in 100 fs of derivative order 10.

should ideally transmit more power at the lower frequencies of the bandwidth which are less affected by the absorption of the channel. The bandwidth B considered is 0.5 to 1.5 THz.

One type of pulse that is possible to fit into the bandwidth is the Gaussian pulse of varying derivative order n and width σ. a_n is the normalization-factor which sets the total energy contained in a pulse to 1 pJ. The Gaussian pulse of derivative order n is defined as:

$$p_n(t) = \frac{d^n}{dt^n}\frac{a_n}{\sqrt{2\pi}\sigma}e^{\frac{-t^2}{2\sigma^2}} \tag{3.6}$$

the Power Spectral Density (PSD) of the Gaussian pulse is $S_n(f) = P_n(f)P_n^*(f)$, where $P_n(f)$ is the Fourier transform of $p_n(t)$ and $P_n^*(f)$ its complex conjugate. It is calculated as:

$$S_n(f) = (2\pi f)^{2n}a_0^2e^{-(2\pi\sigma f)^2}. \tag{3.7}$$

There are two parameters that we may set when designing the pulse. The first parameter is the derivative order n and the other is the standard deviation parameter σ. By increasing n the PSD shifts to the right and attains a more narrow shape. σ influences the time duration of the pulse. Specifcially, lowering it increases the bandwidth of the pulse. The design objective is to maximize the signal-to-noise ratio:

$$SNR = \frac{P_{rx}(r)}{N_m(r)}. \tag{3.8}$$

We also want to ensure that at least 95% of the total power of the pulse $p(t)$ is confined to the bandwidth B to avoid wasting power. This problem can be formulated as:

$$\begin{aligned} &\underset{n,\sigma}{\text{maximize}} \quad SNR \\ &\text{subject to} \quad \int_B S(f)df > 0.95\int_0^\infty S(f)df. \end{aligned} \tag{3.9}$$

A numerical investigation of the SNR was conducted at the distance $r = 1$ mm. For each derivative order n a unique value of σ set to be as large as possible was calculated and the corresponding SNR plotted. The results are given below in Figure 3.4. Note that we were able to evaluate only Gaussian pulses up to order 10 because of numerical instabilities due to large numbers in Matlab.

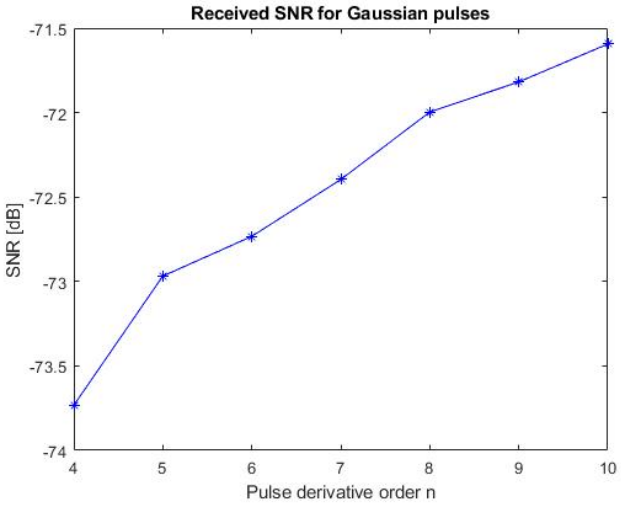

Figure 3.4: The maximum received SNR at 1 mm for pulses containing 1 pJ energy.

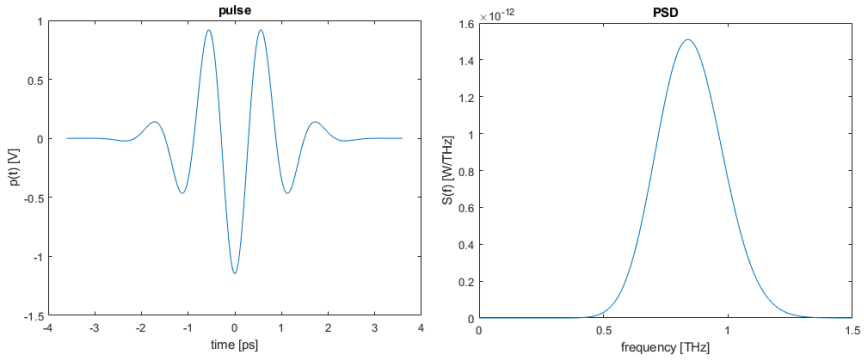

Figure 3.5: This is a $\sigma = 0.6$ ps pulse $p(t)$ of derivative order $n = 10$ containing 1 pJ energy. Its PSD $S(f)$ is shown to the right.

3.5 Receiver Design

An important aspect of every communication system is how to design the detector. The detector is generally more complicated than the transmitter and has to be designed to match the modulation and conditions employed at the nano-scale environment. In general, there are two types of receivers in communication systems: *coherent* and *non-coherent*. The difference between the two detectors is that in coherent detection the receiver takes into account both the amplitude and phase information of the received signal, while in non-coherent detection only the amplitude information of the signal is taken into account. For the purposes of designing a receiver to be used by a NM, a non-coherent receiver is seen as the only feasible option due to the size and technical limitations.

For our purposes, we prefer to design a receiver which does not rely on strict synchronization requirements with another NM. This is because the pulses are so short in time, and the electronics available are unlikely to be able to be set in such an exact way as to allow them to perfectly tune into the short pulses. Therefore, we desire a detector which is able to stay open to listen for pulses for a longer duration of time. Another important system aspect is related to the self-induced noise and how it affects the system performance. This self-induced noise occurs only when transmitting pulses, and it would be desirable to be able to utilize the extra energy of this induced noise to aid in the detection of pulses.

An intuitive solution which fulfills these requirements is an ideal integrator. The ideal integrator integrates the signal over a time interval and whenever the energy is larger than a certain threshold value, it is decided that a pulse was detected.

The non-coherent detector uses the signal $v(t) = |p(t)|^2$ and continuously outputs the value of the integration

$$V(t) = \int_{t}^{t+T} v(\tau) d\tau. \tag{3.10}$$

If at any time during signal reception the integration output is larger than a predetermined threshold level V_T, the detector decides that a pulse was transmitted, otherwise it decides that silence was transmitted. This can be formulated by introducing the peak value $V[n] = max\ V(t),\ 0 < t < T$ and checking if $V[n] > V_T$. How V_T is set is

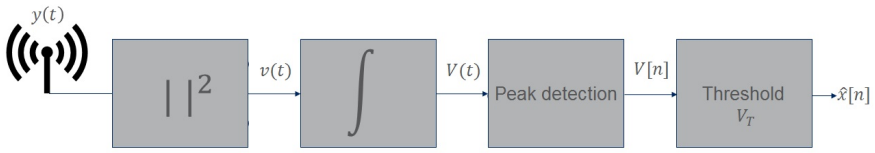

Figure 3.6: Block diagram of the receiver architecture.

discussed in section 3.6.

A practical problem, which arises is that an ideal integrator circuit is too complicated to be realized on a NM. However, it is possible to construct an approximate integrator. Our integrator of choice is an implementation of the one described in [12]. It is realized as a cascade of two RC filters, creating a low-pass filter over our bandwidth of choice. The values of the resistance and capacitance can be made small enough to able to fit onto a NM.

The impulse response of the circuit resembles a pulse and is designed to roughly approximate the square impulse response $i(t)$ an ideal integrator. The detection window is 1σ long and thus it continuously detects the energy of the input signal in the interval of such length. The impulse response $d(t)$ of the detector is:

$$d(t) = z^2 t e^{-zt} \tag{3.11}$$

$z = 1.4615/\sigma$ is used to minimize the mean square error $\int_0^\infty |d(t) - i(t)|^2 dt$. The ideal integrator has the impulse response

$$i(t) = \begin{cases} 1/\sigma, & \text{if } 0 < t < \sigma \\ 0, & \text{otherwise.} \end{cases} \tag{3.12}$$

Both $d(t)$ and $i(t)$ are shown in Figure 3.7. An overall sketch of the receiver design is shown in Figure 3.6.

3.6 Detection Threshold Level

In general, due to the influence of the self-induced noise, when transmitting pulses we will obtain a histogram resembling two Gaussian pulses with different variances.

We may assume that the probability of transmitting a pulse is p_1 and the probability of transmitting silence is $p_0 = 1 - p_1$ and without

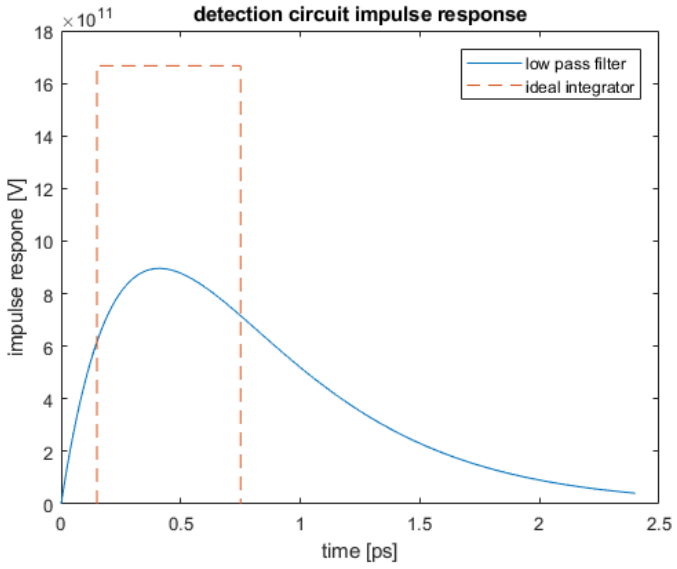

Figure 3.7: The detector impulse response which is trying to mimic the square of an ideal integrator.

loss of generality that $p_0 > p_1$. To minimize the probability of making an erroneous decision $P_e = p_0 \cdot Pr(detect\ 1) + p_1 \cdot Pr(detect\ 0)$ we further assume that

$P \sim \mathcal{N}(\mu_1, \sigma_1^2)$ and $S \sim \mathcal{N}(\mu_0, \sigma_0^2)$. Because there is greater power when transmitting pulses, and the pulses induce extra noise, we may additionally assume that $\mu_0 > \mu_1 > 0$ and $\sigma_1^2 > \sigma_0^2$.

The maximum à posteriori detector (MAP) has two hypotheses θ_0: silence or a zero was transmitted and θ_1: a pulse or one was transmitted. We want to make a decision $\hat{\theta}$ based on the output $V[n]$ of the integrator compered to a threshold level V_T.

$\hat{\theta} = \arg\max_{\theta}; f(x|\theta)g(\theta)$. The function g is the underlying distribution p_0 and p_1.

This detectors threshold level V_T should be at the point

$$\frac{p_1}{\sqrt{2\pi}\sigma_1} e^{-\frac{(V_T-\mu_1)^2}{2\sigma_1^2}} = \frac{p_0}{\sqrt{2\pi}\sigma_0} e^{-\frac{(V_T-\mu_0)^2}{2\sigma_0^2}}, \tag{3.13}$$

which is equivalent to $\frac{p_1\sigma_0}{p_0\sigma_1} = e^{-\frac{(V_T-\mu_0)^2}{2\sigma_0^2} + \frac{(V_T-\mu_1)^2}{2\sigma_1^2}}$. We may simplify this expression further by taking the logarithm of both sides (since it is a monotonically increasing function). We then obtain:

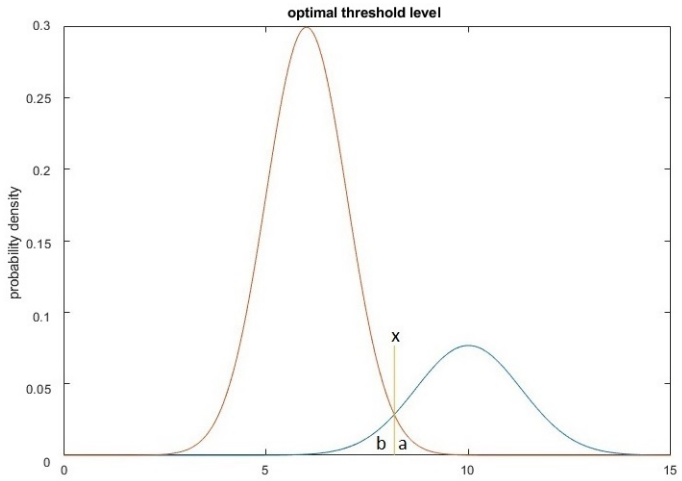

Figure 3.8: The Gaussian probability functions for zeros and ones shown together with crossover probabilities a and b and detection threshold x.

$$ln\left(\frac{p_1\sigma_0}{p_0\sigma_1}\right) > -\frac{(V_T-\mu_0)^2}{2\sigma_0^2} + \frac{(V_T-\mu_1)^2}{2\sigma_1^2}. \tag{3.14}$$

The solution to this inequality is obtained from solving the resulting general second degree equation $x^2 + px + q > 0$ for $p = \frac{2\sigma_1^2\mu_0 - 2\sigma_0^2\mu_1}{\sigma_0^2-\sigma_1^2}$ and $q = \frac{\mu_1^2\sigma_0^2 - \mu_0^2\sigma_1^2 - 2\sigma_1^2\sigma_0^2 ln(\frac{p_1\sigma_0}{p_0\sigma_1})}{\sigma_0^2-\sigma_1^2}$ and throwing away the smallest value solution. Thus, we have:

$$V_T = -\frac{p}{2} + \sqrt{\frac{p^2}{4} - q}. \tag{3.15}$$

One way to calculate the characterizing values of the normal distributions in an actual realization is to transmit a training sequence and make a numerical estimation of the normal distribution parameters based on the received signal.

3.6.1 Binary Asymmetric Channel Model

For our purposes the optimal detector operates over a binary asymmetric channel with crossover probabilities a and b. This model is illustrated in Figure 3.9. The crossover probabilities a, b and the threshold level x obtained from solving the inequality are shown together with two Gaussian distributions in Figure 3.8.

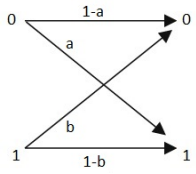

Figure 3.9: The binary asymmetric channel with crossover probabilities a and b.

3.7 Simulation Setup

In this section, we discuss the simulation of the one to one link between two NMs in the human body absent of interference. This is a discrete time simulation of a continuous time system. The simulation approximates how the real continuous time system works by modeling the most essential parts of a communication system. First, a source of bits is loaded into the system and then transmitted one at a time over the channel. Because the pulses are spread in time during transmission over the channel, the received signal contains no inter-symbol interference (ISI). Thus, we are free to transmit and detect each bit independently in our simulation. The system is set up as shown in figure 3.10. The information bit b is loaded, then modulated into a pulse $p(t)$ if $b = 1$ or silence if $b = 0$. The signal is then transmitted and convolved with the channel impulse response $h(t)$. Subsequently, a noise is added to the received signal. The noise power is dependent on we transmitted a zero or a one. If a pulse was transmitted, we add noise of higher power because of the extra self-induced noise contribution. The received signal $y(t)$ can then be expressed as:

$$y(t) = \begin{cases} h(t) * p(t) + n_1(t) & \text{if } b = 1 \\ n_0(t) & \text{if } b = 0 \end{cases} \tag{3.16}$$

$n_0(t)$ is AWGN of zero mean and power N_b, while $n_1(t)$ is AWGN of power $N_b + N_s$ due to the extra induced noise. The received signal $y(t)$ is then sent to the non-coherent detector and approximately integrated by the low-pass filter $d(t)$ as described in section 3.5. A decision is made based on the maximum value D of the integrated signal of the detector, depending on whether it lies above or below the threshold level V_T. Specifically, if $D > V_T$, it decides that a pulse was transmitted.

V_T is set after an initial transmission of $M = 10$ kbits of zeros and

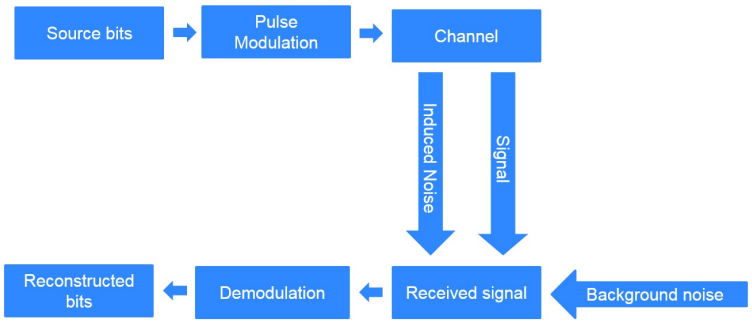

Figure 3.10: The communication link between two NMs.

$M = 10$ kbits of ones have been transmitted and the corresponding receiver output $D = max\ I(t)$ have been noted for the zeros and ones. We then adapt two normal distributions to the data and the threshold level is set as described in described in Section 3.6 using an equal probability $p_0 = p_1 = 0.5$ of transmitting zeros and ones. The relatively large value of M is used to minimize the variations in the normal distribution and reduce the uncertainty in the adapted mean and variance parameters. A histogram of $V[n]$ is shown below in Figure 3.11.

As we are creating a discrete time approximation of the time continuous system, we need to obtain the channel impulse response. This can be done by taking the Inverse Discrete Fourier Transform (IDFT) of the transfer function $H(f)$.

We are creating a simulation of the system at time instances spaced t_s apart. Our goal is to compute a discrete time channel model $h[t_i], i = 0, t_s, 2t_s, ...$, capturing the behavior of the channel. To ensure numerical stability in our computation, we use an $N = 2^{14} = 8192$ point IDFT. Specifically, this IDFT uses frequency-sampling of the channel transfer function $H(f)$ in N points evenly spaced in steps of f_s/N at frequencies ranging from $-f_s/2$ to $f_s/2$.

After a transmission of evenly distributed roughly 100 kbits is complete, we may look at the histogram of the received detected signal to gain further insight into the results. As we can clearly see, the zeros and ones form two distinct peaks roughly resembling two normal distributions, both having their own expectation value and variance. The extra increase in expectation value of the ones stems from the fact that we are receiving and integrating signals with a larger power and we therefore obtain larger output values at the detector. The extra increase

in variance of the ones is because of the larger noise present in the input signal. The integration of this extra noise term adds a greater deal of randomness to the system and is reflected in the histogram. Table 1 gives a detailed list of all the default parameter values used in the simulation.

Table 3.1: Table of default simulation parameters

simulation parameter	**numerical value**
sampling frequency f_s	8 THz
sampling time $T_s = 1/f_s$	0.125 ps
bandwidth B	[0.5, 1.5] THz
total pulse energy	1 pJ
pulse derivative order n	10
pulse standard deviation σ	0.6 ps
pulse length	7.125 ps
channel length	71.25 ps
received signal length	78.375 ps
transmission distance r	2.44 mm
background noise power N_b	4.34 nW or -83.6 dBW
blood refractive index n_0	1.97

3.8 Results

As we decrease the transmission distance, keeping all other parameters of our simulation fixed, we note that the peak in the histogram corresponding to the pulses begins to move, but it also flattens. The increase in expectation value happens because we are receiving more energy on average. The increase in its variance is because of the extra additional self-induced noise the increase in pulse energy produces. We note a similar change if the transmission energy increases. We receive more energy on average, but also a slightly higher degree of induced noise power at the receiver. In Figure 3.11 it is shown how the histogram changes when the transmission distance increases and how it affects the bit error rate (BER). In Figure 3.12, we can see how the BER is affected by transmitting pulses of different energies.

The threshold level has a big influence on the BER, as can be seen

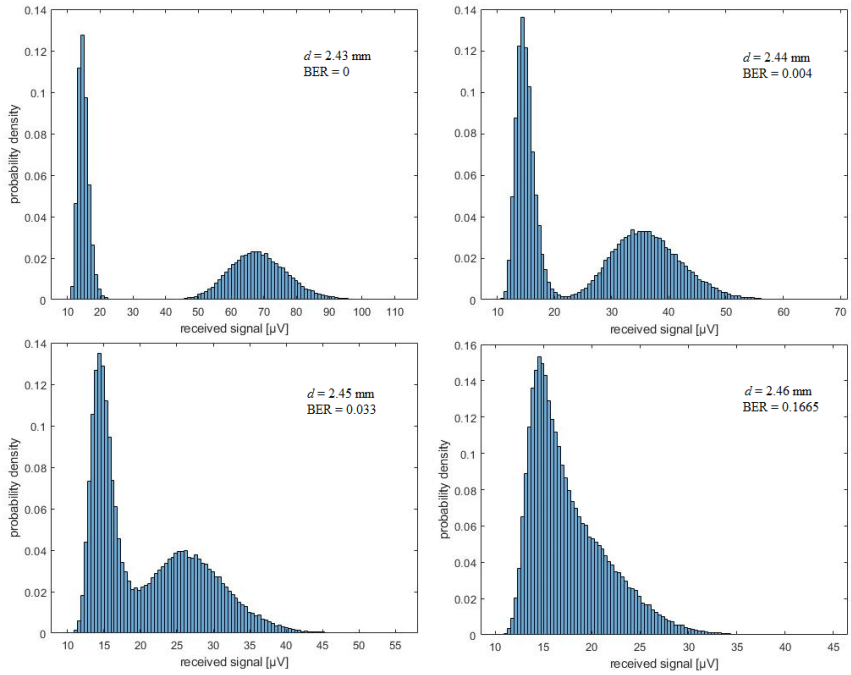

Figure 3.11: Histograms of the received peaks $V[n]$ of a 100 kbit long signal for increasing communication distances (d).

in figure 3.13. By comparing the BER for different threshold levels, we can conclude that approximating the received signal with the normal distribution works well for minimizing the BER. The resulting optimum threshold level calculated from equation (8) is very close to the minimum BER level.

3.9 Conclusions

It was found that Gaussian pulses of derivative order 4 or higher were able to fit 95% of their power within the bandwidth B.

A question one may ask is why integration of a squared Gaussian noise process produces a stochastic output that can be adequately captured by a change in variance in the resulting normal distribution. The answer to this question lies in the Central Limit Theorem, which states that several independent randomly distributed variables become approximately normally distributed as their numbers grow. Our integration is approximately realized as a summation of many stochastic vari-

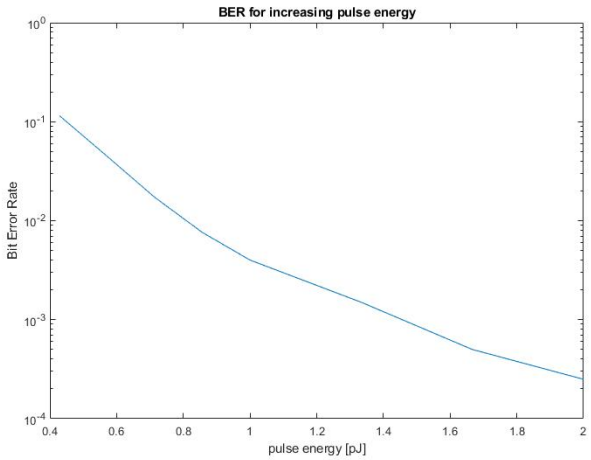

Figure 3.12: The BER for transmitting pulses of different energies at a distance of 2.44 mm.

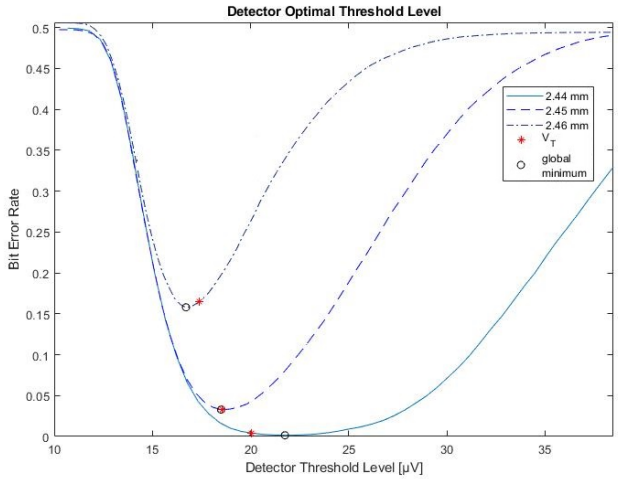

Figure 3.13: The transmission of 30 kbits at a distance of 2.44, 2.45, 2.46 mm and the resulting BER for setting different threshold levels at the detector. The asterisk indicates the position of V_T and the circle the threshold level with minimum BER.

ables. The integration of a noise process squared may be approximated as a summation of several Chi-square distributed random variables. As the noise at different times is uncorrelated, this integration may also be approximated as an additive normally distributed variable. As indicated by 3.13, the normal distribution approximation leading to V_T does a very good albeit not perfect job of estimating the optimal detection threshold level. The main issue is that the distribution of the zeros has a "tail" to the right which cannot adequately be described by the normal distribution, and it results in a threshold level setting which is too low for high SNR cases.

Chapter 4

Nano-Communication Network Design

4.1 Introduction

The small size of the NMs in combination with the high signal absorption at THz frequencies limits the possible communication distance. In order to successfully transmit a message signal over a large distance such as from inside the human body to an external out-of-body device the NMs inside the body have to work together. The objective is to provide the receiver with a better version of the signal through cooperative communication.

4.2 Relaying Schemes

In order to transmit signals over longer distances, we want to investigate using multiple NMs as relays forwarding the signal to increase the probability of having a strong signal reaching the receiver. It is envisioned that the relays will be small nano-devices capable of simple tasks such as amplifying and forwarding (AF) a received signal. The relays are modeled as point sources capable of retransmitting a received signal using a half-duplex time division scheme [7, 14]. This means that each relay will at first stay silent when it receives a signal and then it amplifies and forwards it. This does, however, also mean that any noise in the signal will also be amplified. Because of the substantial path loss, we assume that a transmitted signal is only able to

reach the relay closest to its source [1]. It is assumed that the relays are capable of variable gain forwarding, meaning that they always output signals at a constant power independently of the strength of the signal they receive [8].

The transmission scheme is such that the whole nano-network stays silent during the transmission apart from the relays, when it is their turn to transmit a signal. First, the communicating NM transmits a signal. The receiving relays then amplify and forward their respective received signals to the next relays in line. Accordingly, the envisioned communication scheme looks like:

- a communicating NM transmits a signal.
- the closest relay or relays each receive their own copy of the signal and amplify and forward it.
- the next closest relay or relays receive an amplified and forwarded copy and repeat the process of AF.
- after the chain of AF is complete the target NM receives a copy of the signal from the relay or relays closest to it.

4.3 Topologies

An interesting topic is how to best place the relays. In this regard, several configurations are possible. The simplest topologies are achieved by either placing all of the relays in a cascade between the transmitter and receiver or by placing all the relays equidistant in parallel between the transmitter and receiver. Combinations of relays in a line and in parallel are also possible.

4.3.1 Cascade Relay Network

In the first case we are forwarding a strong received signal multiple times to bridge a larger distance. The structure of a cascade relay setup is illustrated in Figure 4.1. It is the simplest setup we can have, where we are forwarding the signal from one relay to another using one step at a time. The SNR for the received signal γ_K when deploying K relays in cascade is given by:

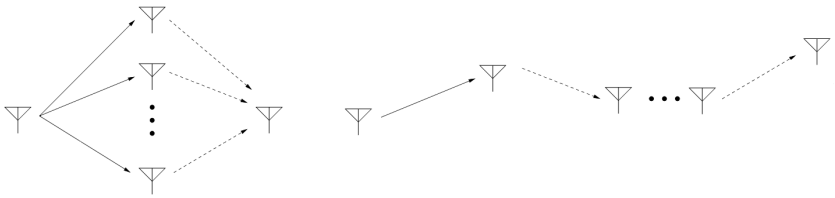

Figure 4.1: Several relays setup in parallel and cascade.

$$\gamma_K = \Big(\prod_{i=1}^{K} (1 + \frac{1}{\gamma_{i,i+1}}) - 1 \Big)^{-1}. \tag{4.1}$$

4.3.2 Parallel Relay Network

In the second configuration, we are instead in providing the receiver with several versions of the signal by placing relays equidistant in between the transmitter and receiver. This arrangement provides a diversity gain, which is illustrated in Figure 4.1. In comparison to the cascade setup, the parallel setup will be transmitting several slightly more distorted versions due to the lower SNR because of the larger communication distance. The communication system uses a maximum ratio combining (MRC) receiver. The resulting SNR at the MRC receiver is given by

$$\gamma_R = \sum_{i=1}^{M} \frac{\gamma_{s,r_i} \gamma_{r_i,d}}{\gamma_{s,r_i} + \gamma_{r_i,d} + 1}. \tag{4.2}$$

As can be seen by definition of γ_R, if all the terms in the sum are on average equal – which they will be given that the transmission power and distances of each relay to its source and destination are equal – the resulting received SNR will on average be directly proportional to the number of relays in the system.

4.3.3 Combination Relay Network

It is possible to combine the idea of having a parallel relay structure with that of a cascade relay structure to setup a chain of several parallel relay structures in a cascade as illustrated in Figure 4.2.

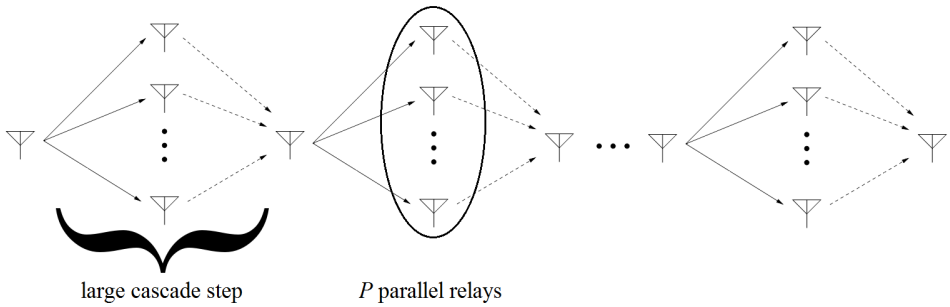

Figure 4.2: A combination of relays in cascade and parallel.

For a relay network between the transmitter and receiver having P relays in parallel and C large cascade steps, where each large step is corresponding to a parallel relay network as shown in figure 4.2, the total number of relays T is equal to the sum of the ones in parallel and the single relays in between. The possible values of T for a combination network depends on the parameters P and C and given by:

$$T = PC + C - 1. \tag{4.3}$$

A list of possible values of T for different values of P and C are shown in Table 4.1.

Table 4.1: Possible number of relays in a topology

relay network topology	**possible number of relays** T
cascade relay network, $P = 1$	any
parallel relay network, $C = 1$	any
combination relay network, $P = 2$	$2, 5, 8, 11, ...$
combination relay network, $P = 3$	$3, 7, 11, 15, ...$
combination relay network, $P = n$	$n, 2n + 1, 3n + 1, ...$

The resulting SNR at the end receiver γ_T is given by combining equation (4.2) with (4.1) – resulting in

$$\gamma_T = \Big(\prod_{j=1}^{2C} (1 + \frac{1}{\gamma_{j,j+1}}) - 1 \Big)^{-1}. \tag{4.4}$$

where

$$\gamma_{j,j+1} = \sum_{i=1}^{P} \frac{\gamma_{s,r_i} \gamma_{r_i,d}}{\gamma_{s,r_i} + \gamma_{r_i,d} + 1}. \tag{4.5}$$

Though here d and s denotes the left and right single relays between the embedded relays in parallel. An interesting observation is that the combination network reduces to a cascade network if $P = 1$ or a parallel network if $C = 1$. For the special case $(P, C) = (1, 1)$ all relay network topologies – combination, cascade and parallel – are equivalent and correspond to the case of deploying a single relay between the transmitter and receiver.

4.4 Simulation Setup

The system parameters investigated are the number of relays and the type network topology. The performance metric used is the probability of having an SNR lower than a certain threshold. If the distance between the transmitter and receiver is large enough (typically a few mm), the signal strength at the receiver will be very low and hard to detect. This is mainly due to the path loss, however we may also have a probability of a signal outage happening. The main task of the relays is to mitigate these effects.

The path loss model is taken from [3]. This is an empirically derived model, based on experimental measurements of collagen used to resemble to propagation conditions of the human skin tissue.

The path loss between two points – either the transmitter s and relay i: r_i or relay i and destination (receiver) d – is denoted l_{s,r_i} and $l_{r_i,d}$ and is calculated using the equations:

$$l_{s,r_i} = -0.2N + 3.98 + (0.44N + 98.48)d_{s,r_i}^{0.65} + (0.068N + 2.4)f^{4.07} \tag{4.6}$$

$$l_{r_i,d} = -0.2N + 3.98 + (0.44N + 98.48)d_{r_i,d}^{0.65} + (0.068N + 2.4)f^{4.07}, \tag{4.7}$$

where $N = 5$ is the number of sweat ducts of the skin containing water which affects propagation conditions. f is the carrier frequency and d_{s,r_i} and $d_{r_i,d}$ are the distances from transmitter to the i_{th} relay and from the i_{th} relay to the destination respectively.

The received SNRs are calculated as $\gamma_{s,r_i} = \frac{|h_{s,r_i}|^2 P_s}{l_{s,r_i}\sigma^2}$ and $\gamma_{r_i,d} = \frac{|h_{r_i,d}|^2 P_s}{l_{r_i,d}\sigma^2}$ where $h_{s,r_i} \sim \mathcal{CN}(0,1)$ and $h_{r_i,d} \sim \mathcal{CN}(0,1)$ are complex normal distributed channel coefficients. Because they only ever occur in this simulation as absolute values squared, they are effectively Chi-square distributed variables with 1 degree of freedom. We have elected to do a numerical study of the system performance. Specifcially, σ^2 is the variance of the additive white Gaussian noise, P_s is the transmit power of the transmitter and P_r is the transmit power of the i_{th} relay. The relays and the transmitter both transmit using 100 nW power. The noise variance per unit bandwidth is -174 dBm/Hz. The system

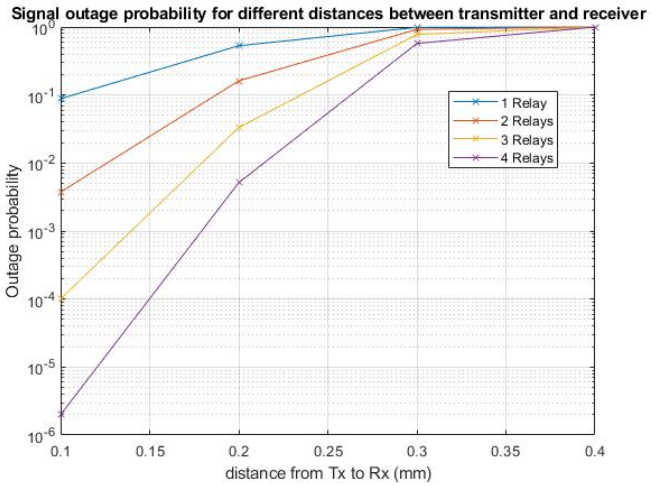

Figure 4.3: Signal outage probability for different distances between transmitter and the receiver. The relays are placed in parallel. The threshold level is set to 10 dB.

bandwidth is set to be 1 GHz, and the carrier frequency is 1 THz. Due to the stochastic nature of the channel coefficients, we are evaluating each signal link multiple times in our simulations. We are using γ_R as our performance metric and are numerically calculating its Cumulative Distribution Function (CDF) to evaluate the system performance.

4.5 Results

In Figure 4.3 we have plotted the outage probability as a function of distance between the transmitter and the receiver for a communication system employing relays all placed midway between the transmitter and receiver. The total distance between the transmitter and receiver varies from 0.1 to 0.4 mm. The path loss is quickly degrading the system performance, as the distance grows.

In Figure 4.4 we can see the outage probability for relays setup in parallel and in Figure 4.5 for relays in cascade. It is interesting to investigate the performance difference between the cascade and parallel setup for a given number of relays. It is shown at a total transmission distance of 0.2 mm in Figure 4.6. The relays in parallel always perform better than the ones in a series for any number of relays.

When comparing a combination network to a parallel for a fixed

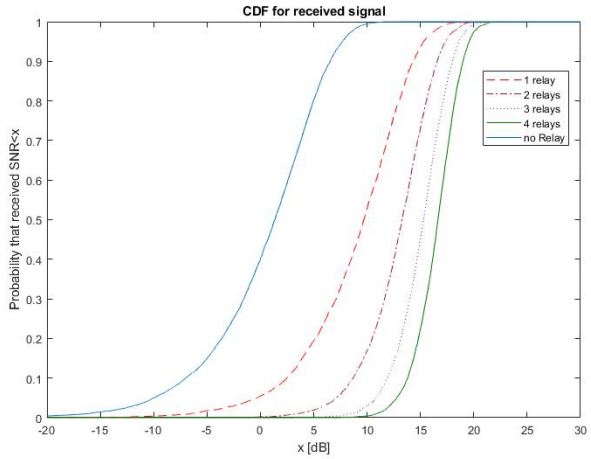

Figure 4.4: Signal outage probability for parallel relay network.

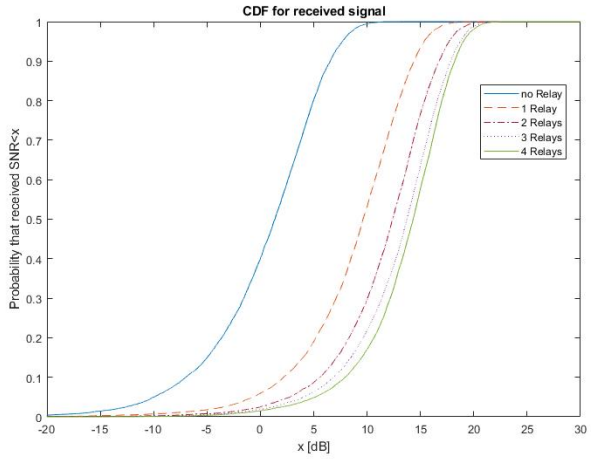

Figure 4.5: Signal outage probability for cascade relay network.

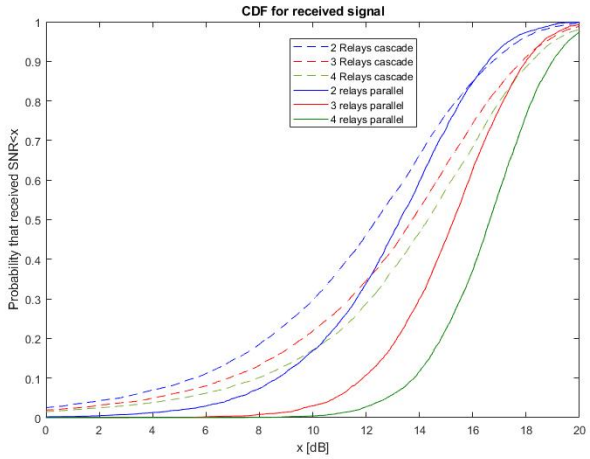

Figure 4.6: Signal outage probability for relays setup in parallel and cascade respectively.

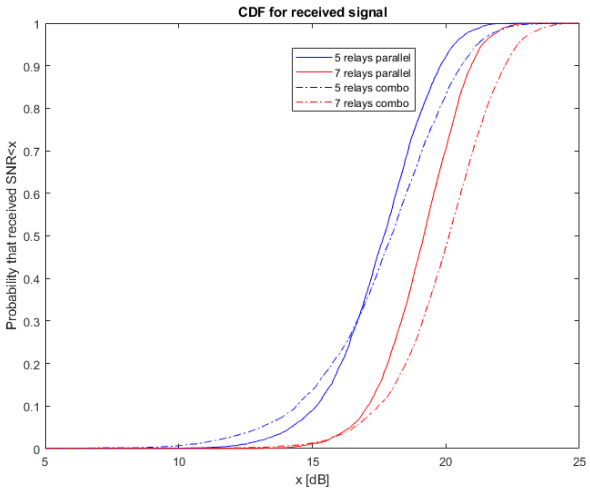

Figure 4.7: Signal outage probability for relays setup in parallel and combination respectively.

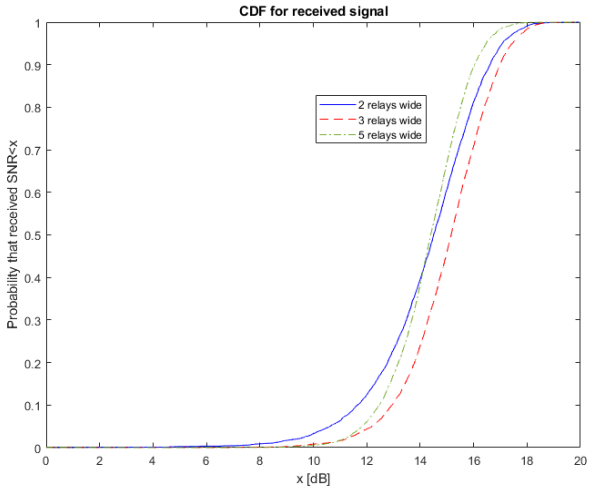

Figure 4.8: Signal outage probability for 11 relays setup in combination networks being 2, 3 or 5 relays wide respectively.

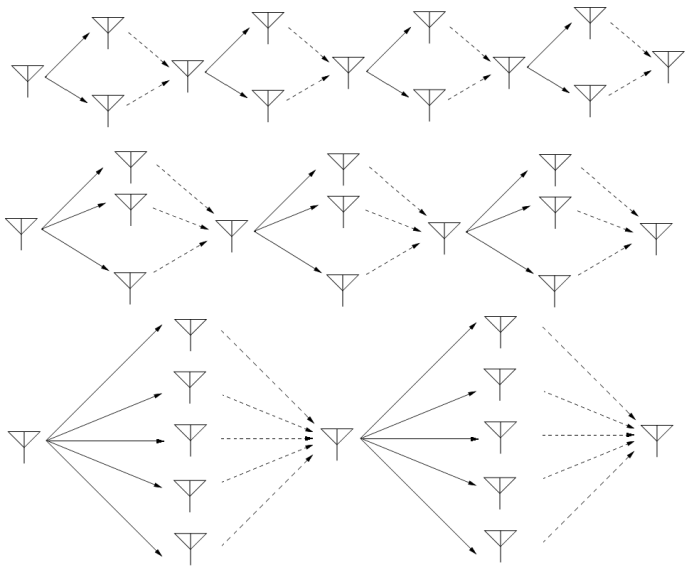

Figure 4.9: 11 relays setup in a combination network for a fixed distance, employing 2, 3 or 5 relays in parallel. Setup values are $(P, C) = (2, 4), (3, 3), (5, 2)$.

distance and number of relays it is interesting to determine when it is better to employ a combination network than a parallel network. The results are shown in Figure 4.7 where deploying 5 relays in a 2 wide combination network and 7 relays in a 3 wide combination network is compared to their parallel counterparts. The performance slightly favors the parallel network compared to the combination network when deploying 5 relays. When 7 relays are used it is clear however that the combination network performs better.

Another important topic is for a given number of relays, how should the combination network best should be set up. We investigated how to best setup 11 relays for a communication distance of $d = 0.4$ mm. This is because 11 is the smallest number able to fit combination networks of three different values of $P = 2, 3$ or 5 as seen in Table 4.1. The different relay setups are shown in Figure 4.9. The performance comparison is shown in Figure 4.8. The result is that the network being 3 relays wide performed better than the network being 2 or 5 relays wide. A related observation is that it is possible to retain the SNR level and transmit the signal a larger distance, when employing a large number of relays in a combination network.

Irrespectively of the setup, we see a great increase in performance when employing relays to forward the signal. Even a single relay yields a great improvement in outage probability as illustrated in Figure 4.5.

4.6 Conclusions

By employing more advanced structures, it is possible to transmit signals further in the body, but the complexity requirements on the NMs also increase. The feasible communication distance can drastically be increased by introducing relays into the system. The average system performance is always better when placing the relays all in between the NMs compared to placing them in a line. There is a mathematical explanation of this phenomenon. When placing the relays in between the NMs, there is always a risk of having a single poor performance link ruining the whole transmission chain. When placing the relays in parallel this risk is significantly reduced. If a certain path is in experiencing a fade, then another is likely working and mitigates the effect. Due to the nature of the MRC receiver, placing another relay in be-

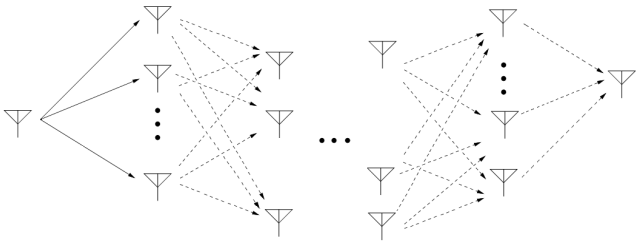

Figure 4.10: An advanced topology utilizing cooperative communication.

tween the transmitter and the receiver always gives a linear increase in the received SNR level, whereas introducing additional relays in the line gives diminishing returns in terms of the received SNR. By combining the two methods, we were however able to increase the performance when more than 5 relays were being used. There are several ways in which the combination network can be set up for a given number of relays – however simulations are needed to evaluate which topology is optimal. We have restricted our analysis to a few simple relay topologies however there is likely that more advanced topologies exist which will perform even better. A sketch of a complex topology is shown in Figure 4.10.

The results obtained in this chapter are not necessarily fully in agreement with the ones in other chapters. This is due to the fact that we are using different channel models and assumptions on NM capabilities. We are also introducing a fading parameter in the channel tap $|h|^2$. This model is built for communication systems using any type of modulation to evaluate the signal performance. The peculiarities of using OOK for nano-communication, such as self-induced noise, are not adequately captured by this model. Nevertheless, it does provide a simplified framework for analyzing and demonstrating the increase in performance of nano communication networks. The increase in performance is valid, even though the exact communication distance and system performance differ.

Chapter 5

Conclusions and Future Works

5.1 Conclusions

The task of designing a fully operational nano-network presents a complex problem with many technical challenges left to tackle. The small size imposes strict requirements on low computational complexity in combination with limited energy storage capabilities. The very large signal absorption rate in the THz band further reduces the feasible communication distance. However, there is also the advantage of deployment in an environment which is free of interference, where one does not have to consider how design choices cause interference to external users. We have seen how we can overcome these challenges (to some extent) by making clever use of modulation, coding and networking solutions. It seems that many solutions have to be adapted to the low complexity and high signal absorption environment in order to work well on the nano scale. In the future, there are likely thousands of NMs densely deployed inside the body. In order to be able to connect the nano-network to an external terminal and transmit important medical information, new models and protocols for cooperative communication will have to be developed. The high signal absorption inside the human body in conjunction with the technical limitations of each NM must be overcome. I believe that the key is to explore novel ideas in cooperative communication between NMs, and utilize their great numbers in order to create a working communication network that in the future will be able to connect to a smartphone and thereby to the cellular ecosystem.

5.2 Future Works

We have restricted our analysis to nano-communication in an environment free of interference. A future study should preferably model the self interference caused by the large number of NMs in the network. Although current measurements are focused around the lower THz bands (0.5-1.5 THz), it would be interesting to investigate the feasibility of NM communications at the higher THz frequencies as well. This is because it has been shown that water molecules experience hindered longitudinal and rotational motion in these regions which are likely to alter the dielectric properties [9]. Other interesting topics include further analysis on how to best design simple energy efficient channel coding schemes and if multi-antenna systems could be used to increase the capabilities of NM communication. An analysis of applicable hardware in the NMs would give valuable new information on the physical capabilities of the NMs themselves. A more detailed framework based on the one-to-one nano link for simulating a larger system of connected NMs would be desirable, especially when exploring how it would be possible to connect the network to an external terminal.

Bibliography

[1] Qammer H Abbasi et al. "Cooperative in-vivo nano-network communication at terahertz frequencies". In: *IEEE Access* 5 (2017), pp. 8642–8647.

[2] Qammer H Abbasi et al. "Nano-communication for biomedical applications: A review on the state-of-the-art from physical layers to novel networking concepts". In: *IEEE Access* 4 (2016), pp. 3920–3935.

[3] Qammer H Abbasi et al. "Terahertz channel characterization inside the human skin for nano-scale body-centric networks". In: *IEEE Transactions on Terahertz Science and Technology* 6.3 (2016), pp. 427–434.

[4] Nazim Agoulmine et al. "Enabling communication and cooperation in bio-nanosensor networks: toward innovative healthcare solutions". In: *IEEE Wireless Communications* 19.5 (2012).

[5] Youssef Chahibi, Ian F Akyildiz, and Ilangko Balasingham. "Propagation modeling and analysis of molecular motors in molecular communication". In: *IEEE transactions on nanobioscience* 15.8 (2016), pp. 917–927.

[6] Hadeel Elayan et al. "Photothermal Modeling and Analysis of Intrabody Terahertz Nanoscale Communication". In: *IEEE transactions on nanobioscience* 16.8 (2017), pp. 755–763.

[7] M. Fallgren, G. Fodor, and P. Skillermark. "Wireless Devices, Network Node and Methods for Handling Relay Assistance in a Wireless Communications Network". 2014/0171062 A1. 2014.

[8] Golnaz Farhadi and Norman C Beaulieu. "A general framework for symbol error probability analysis of wireless systems and its application in amplify-and-forward multihop relaying". In:

IEEE Transactions on Vehicular Technology 59.3 (2010), pp. 1505–1511.

[9] Matthias Heyden et al. "Dissecting the THz spectrum of liquid water from first principles via correlations in time and space". In: *Proceedings of the National Academy of Sciences* 107.27 (2010), pp. 12068–12073.

[10] Josep Miquel Jornet and Ian F Akyildiz. "Channel modeling and capacity analysis for electromagnetic wireless nanonetworks in the terahertz band". In: *IEEE Transactions on Wireless Communications* 10.10 (2011), pp. 3211–3221.

[11] Josep Miquel Jornet and Ian F Akyildiz. "Femtosecond-long pulse-based modulation for terahertz band communication in nanonetworks". In: *IEEE Transactions on Communications* 62.5 (2014), pp. 1742–1754.

[12] Josep Miquel Jornet, Ian F Akyildiz, et al. "Fundamentals of electromagnetic nanonetworks in the terahertz band". In: *Foundations and Trends® in Networking* 7.2-3 (2013), pp. 77–233.

[13] Janko Katic. "Efficient Energy Harvesting Interface for Implantable Biosensors". PhD thesis. KTH, 2015.

[14] M. Kazmi and G. Fodor. "Relaying in Mixed Licensed and Unlicensed Carrier Aggregation". 8995331 B2. 2015.

[15] Nima N Moghadam, Hamed Farhadi, and Mats Bengtsson. "An energy efficient communication technique for medical implants/micro robots". In: *Medical Information and Communication Technology (ISMICT), 2016 10th International Symposium on*. IEEE. 2016, pp. 1–5.

[16] Tadashi Nakano et al. "Molecular communication and networking: Opportunities and challenges". In: *IEEE transactions on nanobioscience* 11.2 (2012), pp. 135–148.

[17] Rui Zhang et al. "Analytical characterisation of the terahertz in-vivo nano-network in the presence of interference based on TS-OOK communication scheme". In: *IEEE Access* 5 (2017), pp. 10172–10181.

[18] Rui Zhang et al. “Analytical modelling of the effect of noise on the terahertz in-vivo communication channel for body-centric nano-networks”. In: *Nano communication networks* 15 (2018), pp. 59–68.

[19] Rui Zhang et al. “Modelling of the terahertz communication channel for in-vivo nano-networks in the presence of noise”. In: *Microwave Symposium (MMS), 2016 16th Mediterranean*. IEEE. 2016, pp. 1–4.

TRITA EECS-EX-2018:666